

Probing the QCD phase structure using event-by-event fluctuations

Tapan K. Nayak

CERN, CH-1211, Geneva 23, Switzerland, and
National Institute of Science Education and Research, HBNI, Bhubaneswar, India

E-mail: Tapan.Nayak@cern.ch

Abstract. Heavy-ion collisions at relativistic energies probe matter at extreme conditions of temperatures and energy densities. The study of event-by-event fluctuations of experimental observables is crucial to probe the QCD phase transition, locate the critical point, and learn about the associated critical phenomena. At the critical point, all thermodynamic quantities behave anomalously. Fluctuation measurements provide access to thermodynamic response functions. We discuss the methods for obtaining the isothermal compressibility using particle multiplicity fluctuation, and specific heat using fluctuations in mean transverse momentum, temperature, and energy. Lattice QCD calculations have predicted non-monotonic behavior in the higher-order cumulants of conserved quantities at the critical point. Fluctuations in the multiplicity of charged to neutral particles have been measured to understand the formation of domains of disoriented chiral condensates. We review the recent fluctuation results as a function of collision centrality and energy from experiments at SPS, RHIC, and LHC. In addition, we propose to map the temperature fluctuations in η - ϕ plane to probe local fluctuations of temperature and energy density.

1. Introduction

According to the theory of Quantum Chromo Dynamics (QCD), under extreme conditions of temperatures and energy densities, normal hadronic matter goes through a phase transition to a system of deconfined quarks and gluons, the quark-gluon plasma (QGP). The QCD phase structure between these two distinct states of matter span a wide range of baryon chemical potential (μ_B) and temperature (T) as shown in Fig. 1. Lattice QCD calculations indicate that at vanishing μ_B , the transition from the QGP to a hadron gas is a smooth crossover [1, 2, 3, 4], while at large μ_B , the phase transition is of first order [5, 6]. The point in T and μ_B where the first order transition ends and instigates a crossover transition is denoted as the QCD critical point. Theoretical and experimental studies explore the rich landscape of the QCD phase diagram to understand the nature of the phase transition, locate the critical point, and to learn about the properties of the matter formed.

The experimental program to study the QCD phase structure started more than three decades ago at Bevelac, Berkeley and since then has covered four generations of experiments at the Brookhaven National Laboratory (BNL) and CERN. The collisions at the Large Hadron Collider (LHC) and at the top energy at the Relativistic Heavy Ion Collider (RHIC) probe the conditions at low μ_B . The beam energy scan (BES) program at RHIC [7, 8] is specially designed to probe the location of the critical point by varying the collision energy at close intervals in T - μ_B . In

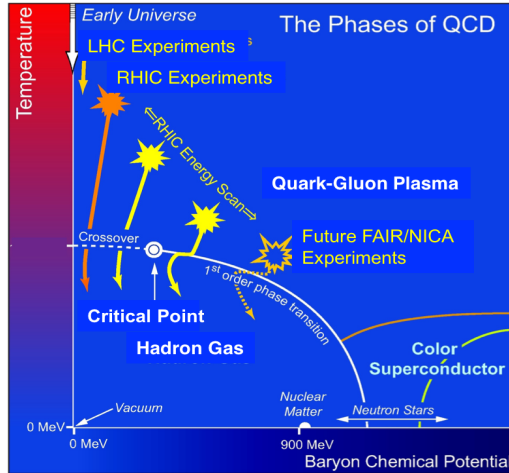


Figure 1. A schematic QCD phase diagram in the temperature (T) and baryonic chemical potential (μ_B) plane. The regions probed by different accelerator facilities are indicated.

future, this program will be complemented by upcoming facilities at Dubna, Russia, and GSI, Germany to explore large μ_B regions in the phase diagram. The regions probed by different accelerator facilities are indicated in Fig. 1.

Fluctuations play a crucial role in the study of phase transition and any associated critical phenomena. Event-by-event fluctuations in a number of observables have been predicted as signatures of the QCD phase transition and the critical point [9, 10, 11]. Several thermodynamic quantities show varying fluctuation patterns when the system goes through the phase boundary. The defining characteristics of the QCD phase transition are the abrupt changes in the physical properties of the system which can be inferred through the analysis of fluctuations of different observables. At the critical point, the fluctuations are expected to be very large. The main fluctuation signatures emanate in the form of event-by-event measurement in the number of particles, momenta of particles, as well as the spatial and energy driven patterns of multiplicity distributions. In this article, we discuss some of the fluctuation techniques, experimental results, and future prospects.

- Thermodynamic response functions: Response functions such as isothermal compressibility (k_T), specific heat (c_v), and speed of sound, are related by the equation of state (EOS), which governs the evolution of the system. The nature of phase transitions in a system can be understood by the measurement of thermodynamic response functions. These quantities can be accessed experimentally by the fluctuation of measured quantities. The heat capacity is related to the fluctuations in temperature [12, 13], whereas in the grand canonical ensemble (GCE) framework k_T is related to the fluctuation in particle multiplicity [14]. Skewness of mean transverse momentum ($\langle p_T \rangle$) fluctuations has recently been proposed as a probe of hydrodynamic behavior in nuclear collisions [15]. By measuring the event-by-event fluctuations in particle multiplicity (N), $\langle p_T \rangle$, and mean transverse energy, we can get access to the response functions.
- Fluctuations of conserved quantities: Lattice QCD calculations reveal that the higher order cumulants of conserved quantities, such as net-charge (Q), net-proton (B), and net-strangeness (S), within a limited acceptance, are proportional to the powers of the correlation length and are expected to diverge at the critical point [16, 17]. Experimentally, it is possible to measure Q , B , and S on an event-by-event basis and obtain the cumulants

of these distributions. In addition, off-diagonal cumulants explore the flavor carrying susceptibilities of the system [18, 19, 20, 21]. Assuming that the signal at freeze-out survives dissipation during the evolution of the fireball from the hadronization stage, the higher cumulants can be used as one of the preferred tools for locating the critical point.

- Disoriented chiral condensates (DCC): Disoriented chiral condensates (DCC), localized in phase space, have been predicted to be formed in high energy heavy-ion collisions when the chiral symmetry is restored at high temperatures [22, 23]. Anomalous event-by-event fluctuations of the neutral to charged pions as well as neutral to charged kaons have been predicted as signatures of the formation of DCC. A fresh look at RHIC and LHC energies is needed to infer about the formation of the DCC domains.
- Fluctuation map: The physics of heavy-ion collisions at ultra-relativistic energies has often been compared to the Big Bang phenomenon of the early Universe. Observation of the cosmic microwave background radiation (CMBR) by various satellites confirms the Big Bang evolution, and inflation; that provides important information regarding the early Universe and its evolution with excellent accuracy. The matter produced at extreme conditions of energy density and temperature in heavy-ion collisions is a Big Bang replica on a tiny scale [24, 25, 26]. We propose to map the temperature fluctuations in η - ϕ plane to probe local fluctuations of temperature and energy density.

2. Multiplicity fluctuation and estimation of isothermal compressibility

Isothermal compressibility (k_T) is the measure of the relative change in volume with respect to change in pressure [14],

$$k_T|_{T,\langle N \rangle} = -\frac{1}{V} \left(\frac{\partial V}{\partial P} \right) \Big|_{T,\langle N \rangle} \quad (1)$$

where V, T, P represent volume, temperature, and pressure of the system, respectively, and $\langle N \rangle$ stands for the mean yield of the particles. In the Grand Canonical Ensemble (GCE) framework, the variance of the number of particles is directly related to k_T :

$$\omega_{\text{ch}} = \frac{k_B T \langle N \rangle}{V} k_T, \quad (2)$$

where ω_{ch} is the scaled variance of multiplicity distribution. This formalism may be applied to experimental measurements of multiplicity at mid-rapidity, as energy and conserved quantum numbers are exchanged with the rest of the system.

At the chemical freeze-out surface, the inelastic collisions cease, and thus the hadron multiplicities get frozen. While the ensemble average thermodynamic properties like the temperature and volume can be extracted from the mean hadron yields, k_T can be accessed through the measurements of the event-by-event multiplicity fluctuations. This has been explored in Ref. [27] and the estimated values of k_T are shown in Fig. 2 for available experimental data and estimations from the HRG calculations. The HRG calculations reveal a sharp increase in the value of k_T around $\sqrt{s_{\text{NN}}} \sim 20$ GeV. It will be interesting to explore the behavior of k_T at BES-II energies and future facilities.

3. Temperature and $\langle p_T \rangle$ fluctuations and estimation of specific heat

Heat capacity (C) is a response function which expresses how much the temperature of a system changes when the heat is transferred to it. The specific heat (c_v) is heat capacity divided by the number of charged particles. Equivalently, for a system in thermal equilibrium to a bath at

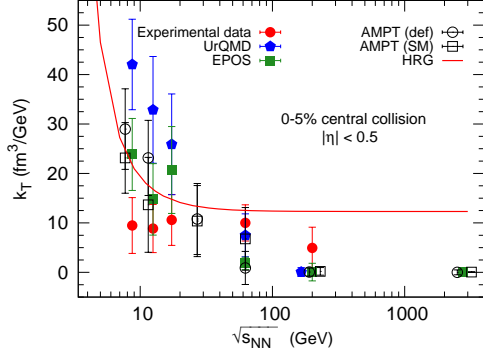


Figure 2. Isothermal compressibility, k_T as a function of collision energy for central collisions [27].

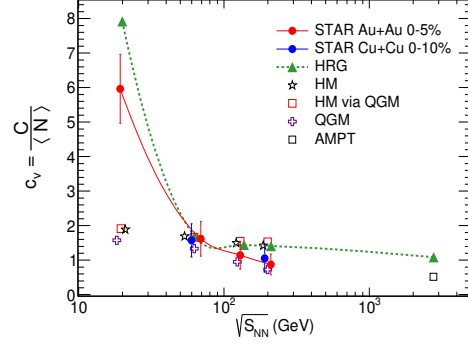


Figure 3. Specific heat, c_v as a function of collision energy for central collisions [28].

temperature, T , we can write [12, 13]:

$$C = \left(\frac{\partial E}{\partial T} \right)_V = \frac{\langle E^2 \rangle - \langle E \rangle^2}{\langle T^2 \rangle}. \quad (3)$$

where V and E are volume and energy of the system, respectively. By expressing the transverse momentum spectra of emitted particles in terms of event-by-event temperature fluctuation ($\Delta T = T - \langle T \rangle$), we obtain:

$$P(T) \sim \exp\left[-\frac{C}{2} \frac{(\Delta T)^2}{\langle T \rangle^2}\right], \quad \frac{1}{C} = \frac{\langle T^2 \rangle - \langle T \rangle^2}{\langle T \rangle^2}. \quad (4)$$

Heat capacity thus can be estimated from the fluctuations in energy or temperature. For a system in equilibrium, the mean values of T and E are related by an equation of state. However, the fluctuations in energy and temperature have very different behavior. Energy being an extensive quantity, its fluctuation has a volume dependent component. So energy is not suited for obtaining the heat capacity. On the other hand, temperature fluctuations provide a good major for the estimation of specific heat. The temperature of the system can be obtained from the transverse momentum (p_T) spectra of the emitted particles. For a range of p_T within a to b , we obtain [28]:

$$\langle p_T \rangle = \frac{\int_a^b p_T^2 F(p_T) dp_T}{\int_a^b p_T F(p_T) dp_T} = 2T_{\text{eff}} + \frac{a^2 e^{-a/T_{\text{eff}}} - b^2 e^{-b/T_{\text{eff}}}}{(a + T_{\text{eff}})e^{-a/T_{\text{eff}}} - (b + T_{\text{eff}})e^{-b/T_{\text{eff}}}}. \quad (5)$$

This equation links the value of event-by-event $\langle p_T \rangle$ within a specified range of p_T to the apparent or effective temperature (T_{eff}). The dynamical component of the $\langle p_T \rangle$ and T distributions have been obtained for RHIC energies after subtracting the corresponding mixed event distributions. The heat capacity is calculated using the dynamical part of the fluctuation and the kinetic temperature. In Ref. [28], $\langle p_T \rangle$ results from the STAR collaboration have been used to calculate heat capacity. The results of the specific heat as a function of collision energy are presented in Fig. 3. It shows a sharp rise in c_v below $\sqrt{s_{\text{NN}}} = 62.4$ GeV. In order to probe the QCD critical point, a finer scan of beam energy at RHIC is essential.

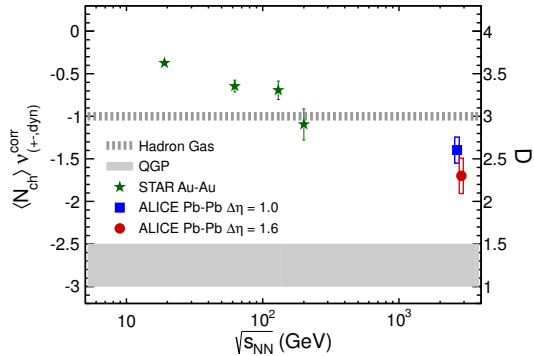


Figure 4. Collision energy dependence of the net-charge fluctuations in central collisions [29].

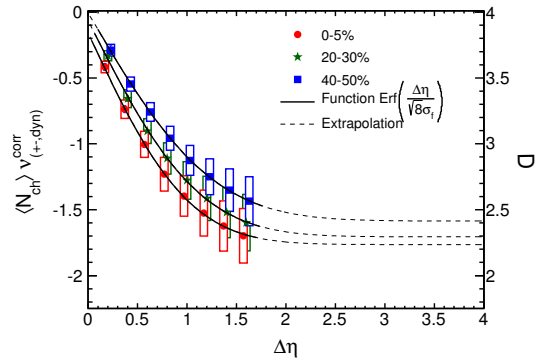


Figure 5. Growth of net charge fluctuations as a function of the pseudorapidity window ($\Delta\eta$) [29].

4. Dynamical net-charge fluctuations

Net-charge fluctuations are strongly dependent on which phase the fluctuations originate. This is because, in the QGP phase, the charge carriers are quarks with fractional charges, whereas the particles in a hadron gas carry a unit charge. The fluctuations in the net charge depend on the squares of the charge states present in the system, and so, the net-charge fluctuations in the QGP phase are significantly smaller compared to that of a hadron gas. The initial QGP phase is strongly gluon dominated, and so the fluctuation per entropy may further be reduced as the hadronization of gluons increases the entropy. The charge fluctuations are best studied by calculating the quantity $\nu_{(+-, \text{dyn})}$, defined as:

$$\nu_{(+-, \text{dyn})} = \frac{\langle N_+(N_+ - 1) \rangle}{\langle N_+ \rangle^2} + \frac{\langle N_-(N_- - 1) \rangle}{\langle N_- \rangle^2} - 2 \frac{\langle N_- N_+ \rangle}{\langle N_- \rangle \langle N_+ \rangle}, \quad (6)$$

which is a measure of the relative correlation strength of particle pairs. A negative value of $\nu_{(+-, \text{dyn})}$ signifies the dominant contribution from correlations between pairs of opposite charges. The $\nu_{(+-, \text{dyn})}$ has been found to be robust against random efficiency losses. It is related to the fluctuation measure (D) by:

$$\langle N_{\text{ch}} \rangle \nu_{(+-, \text{dyn})} \approx D - 4, \quad (7)$$

$$\text{where } D = 4 \frac{\langle \delta Q^2 \rangle}{\langle N_{\text{ch}} \rangle}. \quad (8)$$

Here $Q = N_+ - N_-$, and $N_{\text{ch}} = N_+ + N_-$. Figure 4 shows the values of $\langle N_{\text{ch}} \rangle \nu_{(+-, \text{dyn})}^{\text{corr}}$ as a function of collision energy, measured by the STAR and ALICE Collaborations [29, 30]. Here $\nu_{(+-, \text{dyn})}$ is corrected for global charge conservation and finite detector acceptance. A monotonic decrease in the value of D , measured has been observed.

The measured fluctuations get diluted during the evolution of the system from hadronization to kinetic freeze-out because of the diffusion of charged hadrons in rapidity [31, 32, 33]. This has been studied by plotting dependence of net-charge fluctuations on the width of the rapidity window as shown in Fig. 5 for Pb-Pb collisions at $\sqrt{s_{\text{NN}}} = 2.76$ TeV. We observe that for a given centrality bin, the D -measure shows a strong decreasing trend with the increase of $\Delta\eta$. In fact, the curvature of D has a decreasing slope with a flattening tendency at large $\Delta\eta$ windows. The data points are fitted with a functional form, $\text{erf}(\Delta\eta/\sqrt{8}\sigma_f)$, which represents the diffusion in

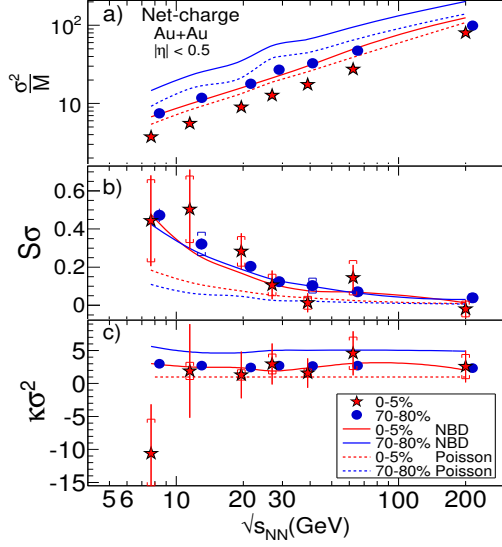


Figure 6. Collision energy dependence of the net-charge fluctuations in central collision [35].

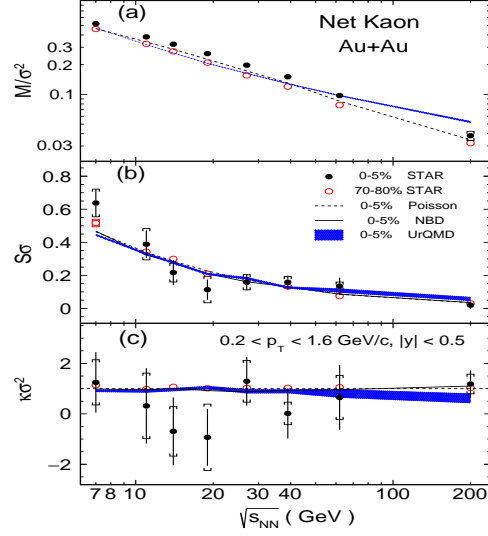


Figure 7. Collision energy dependence of the net-kaon fluctuations in central collisions [36].

rapidity space. The value of σ_f , which represents the diffusion at freeze-out, turns out to be 0.41 ± 0.05 for central collisions. Taking the dissipation into account, the asymptotic value of fluctuations may represent the primordial fluctuations. It would be intriguing to make this study for a wider $\Delta\eta$ range in which most of the fluctuations are captured [34].

5. Fluctuations of conserved quantities: diagonal cumulants

Lattice QCD calculations have shown that higher order cumulants of the distributions of conserved charges are related to the corresponding higher-order thermodynamic susceptibilities and to the correlation length (ξ) of the system. These cumulants go through rapid changes near the critical point. Thus the measurement of cumulants of Q , B , and S provide a direct correspondence to the lattice calculations and serve as an important probe for the critical point search.

The event-by-event distributions of the conserved quantities within a limited acceptance are characterized by mean (M), standard deviation (σ), skewness (S), kurtosis (κ), and other higher order cumulants. The products of the moments, such as σ^2/M , $S\sigma$, and $\kappa\sigma^2$ are constructed to cancel the volume term. The net-charge multiplicity distributions directly probe the charge quantum number, whereas the net-proton and net-kaon distributions provide good proxies for the net-baryon and net-strangeness conserved quantities.

The STAR Collaboration has made extensive measurements of the cumulants of net-charge, net-kaon, and net-proton multiplicity distributions in Au–Au collisions at a wide range of energies starting from $\sqrt{s_{NN}}=7.7$ GeV to 200 GeV. The collision centrality and energy dependence of the products of moments have been reported in a series of publications. Here we reproduce some of the salient features of the recent results.

The results of the cumulants of net-charge multiplicity distributions [35] for $|\eta| < 0.5$ are shown in Fig. 6. Weak centrality dependence is observed for both $S\sigma$ and $\kappa\sigma^2$ at all energies. However, within the present uncertainties, no non-monotonic behavior as a function of collision energy. The net-kaon results [36] are shown in Fig. 7. The collision energy dependence of

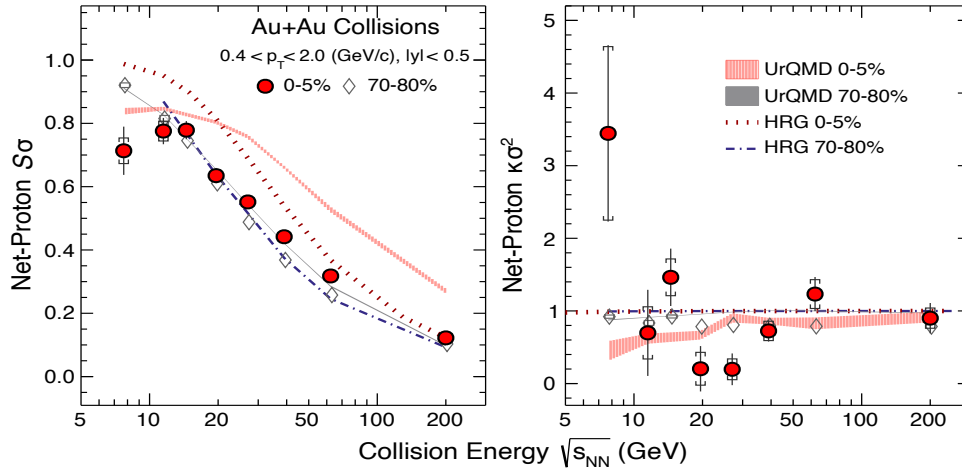


Figure 8. Collision energy dependence of the net-proton fluctuations in central and peripheral collisions [37].

products of cumulants is seen to be smoothly varying as a function of collision energy. No significant collision centrality dependence is observed for both M/σ^2 and $S\sigma$ at all energies. Although the collision centrality and energy dependence of $\kappa\sigma^2$ look very intriguing, no definitive statement can be made within the current experimental uncertainties.

The experimental results of the net-proton multiplicity distributions have been reported in Ref. [37, 38, 39], and summarized in Fig. 8. The collision energy dependence of $S\sigma$ shows a smooth variation as a function of energy except at very low energies. On the other hand, the nature of $\kappa\sigma^2$ variation is very different. For peripheral collisions, there is no variation with energy, whereas a non-monotonic variation (with 3.0σ significance) with beam energy is observed for $\kappa\sigma^2$. This variation could not be explained by hadron resonance gas (HRG) calculation and the UrQMD transport model simulation. This observation is most likely compatible with the theoretical predictions of the critical point. This signature has not been observed in other observables so far.

STAR collaboration has recently reported the beam energy dependence of net- Λ cumulants [40], which is potentially interesting towards our comprehensive understanding of particle production mechanisms and their correlations as Λ carry both baryon and strangeness quantum number. Results of this challenging measurement in terms of the beam energy dependence of the ratios of first, second and third order cumulants are shown in Fig. 9, which show no non-monotonic behavior for the energies and cumulants studied. These results are important for the understanding of the freeze-out temperature in the context of both baryon number and strangeness conservation.

6. Off-diagonal cumulants of conserved quantities

The diagonal and off-diagonal susceptibilities of second order can be expressed in terms of second order central moments (σ):

$$\begin{pmatrix} \sigma_Q^2 & \sigma_{QB}^{1,1} & \sigma_{QS}^{1,1} \\ \sigma_{BQ}^{1,1} & \sigma_B^2 & \sigma_{BS}^{1,1} \\ \sigma_{SQ}^{1,1} & \sigma_{SB}^{1,1} & \sigma_S^2 \end{pmatrix}$$

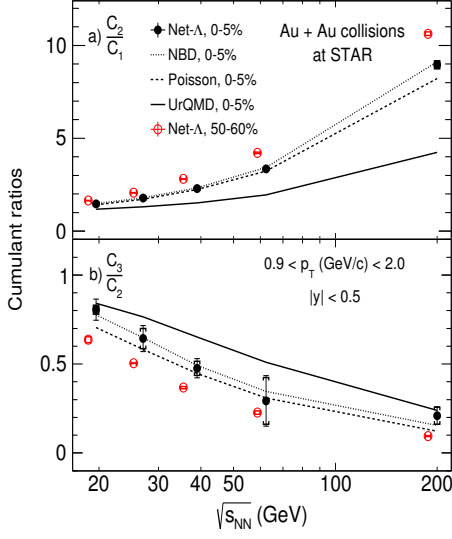


Figure 9. Beam energy dependence of net- Λ cumulant ratios, C_2/C_1 , and C_3/C_2 in most central and peripheral Au–Au collisions [40].

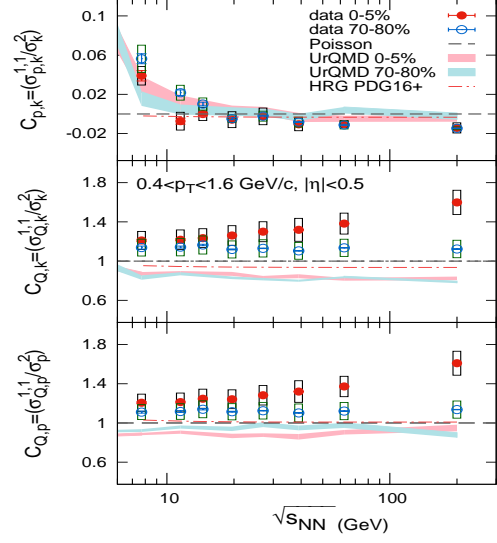


Figure 10. Beam energy dependence of cumulant ratios $C_{p,k}$, $C_{Q,k}$, and $C_{Q,p}$, of net-proton, net-kaon and net-charge for Au–Au collisions [41].

The measurement of these observables give information on the flavor carrying susceptibilities.

The ratios of diagonal and off-diagonal elements are constructed to cancel the volume effect. In the quasiparticle picture of quarks and gluons, the ratios χ_{BS}^{11}/χ_S^2 and χ_{QS}^{11}/χ_S^2 are $-1/3$ and $1/3$, respectively. Other ratios, like χ_{QB}^{11}/χ_B^2 has no contribution from both light and strange quarks. Thus the following ratios are constructed:

$$C_{BS} = -3 \frac{\chi_{BS}^{11}}{\chi_S^2}, \quad C_{SB} = -\frac{1}{3} \frac{\chi_{BS}^{11}}{\chi_B^2}, \quad (9)$$

$$C_{QS} = 3 \frac{\chi_{QS}^{11}}{\chi_S^2}, \quad C_{SQ} = \frac{\chi_{QS}^{11}}{\chi_Q^2}, \quad (10)$$

$$C_{QB} = \frac{\chi_{QB}^{11}}{\chi_B^2}, \quad C_{BQ} = \frac{\chi_{QB}^{11}}{\chi_Q^2}. \quad (11)$$

Beam energy dependence of the ratios ($C_{p,k}$, $C_{Q,k}$, and $C_{Q,p}$) [41] are shown in Fig. 10 for central and peripheral collisions. The values of $C_{p,k}$ are negative at 200 GeV, and change sign around 19.6 GeV for most central collisions. Both $C_{Q,p}$ and $C_{Q,k}$ show strong centrality dependence indicating the presence of a large excess correlation in central events in comparison with peripheral events. In addition, the strong dependence of the cumulants is observed with the phase space window of measurements. With higher statistics datasets and improved acceptance of the STAR detector during the second phase of the BES program (BES-II) it will be possible to measure higher-order off-diagonal cumulants.

7. Exploring the formation of DCC domains

The DCC domains are expected to emit pions coherently from the collision volume, resulting in large fluctuations in the fraction of charged to neutral pions. The neutral pion fraction for

DCC domains is predicted to follow a probability distribution of the form $P(f) = 1/2\sqrt{f}$, which is different from normal events. Heavy-ion experiments at the CERN SPS [42, 43, 44, 45] have put upper limits on the DCC formation as shown Fig 11, whereas anomalous fluctuations have been reported at RHIC [46]. A fresh look at RHIC and LHC energies using both pion and kaon sectors [47] is needed to infer about the formation of the DCC domains.

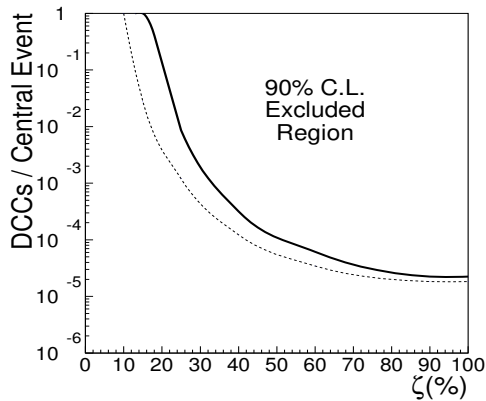


Figure 11. 90% C.L upper limit on DCC production per central event in 158 AGeV Pb–Pb Collisions as a function of the fraction of DCC pions[43].

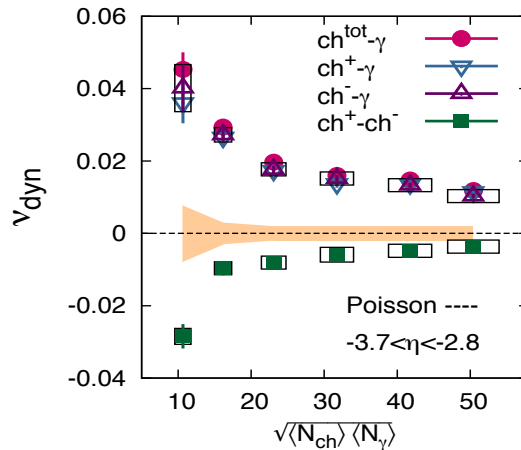


Figure 12. Dynamical correlation between positive and negative charged particles in Au–Au collisions at $\sqrt{s_{NN}}=200\text{GeV}$ [46].

8. Mapping the little bang: local fluctuations

In little bangs, the produced fireball goes through a rapid evolution from an early state of partonic quark-gluon plasma (QGP) to a hadronic phase and finally freezes out within a few tens of fm. Heavy-ion experiments are predominantly sensitive to the conditions that prevail at the later stage of the collision as majority of the particles are emitted near the freeze-out. As a result, a direct and quantitative estimation of the properties of hot and dense matter in the early stages and during each stage of the evolution has not yet been possible.

Relativistic hydrodynamic calculations reveal fluctuations of initial energy density and temperature, which may survive till the freeze-out. Initial fluctuating conditions have been found to be necessary for explaining observed elliptic flow in central collisions and substantial triangular flow of charged particles [25]. The initial state fluctuations may have their imprint on the bin to bin local fluctuations within an event. Event-by-event hydrodynamic calculations provide a strong theoretical basis for studying the global and local fluctuations in ϵ and T [48]. The local fluctuations have been quantified throughout the evolution by simulating central Pb–Pb events at LHC energy by the use of a (2+1)-dimensional event-by-event ideal hydrodynamical framework with lattice-based EOS [25].

In Fig. 13, we present distributions of ϵ and T in the transverse plane at four proper times (τ). At early times, sharp and pronounced peaks in ϵ and hotspots in T are observed. Large bin-to-bin fluctuations observed in ϵ and T indicate that the system formed immediately after collision is quite inhomogeneous in phase space. As time elapses, the system cools, expands, and the bin-to-bin variations in ϵ and T become smooth. These observations are quantified in terms of the average over all the bins and bin to bin fluctuations in ϵ and T , plotted as a function of τ , shown in Fig. 14. We observe that ϵ decreases sharply up to $\tau = 1$ fm, and then the decrease

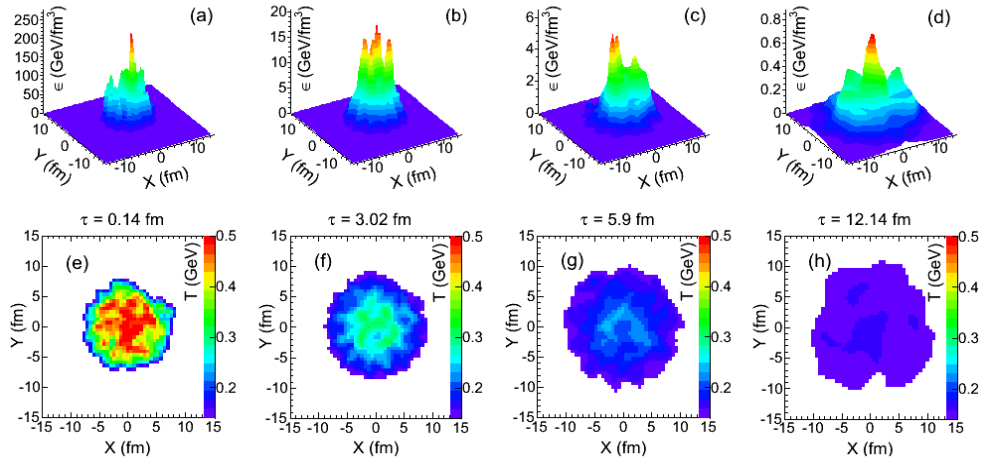


Figure 13. Hydrodynamic calculations of energy density (upper panels) and temperature (lower panels) in the transverse plane for a single Pb–Pb event at LHC energy [48].

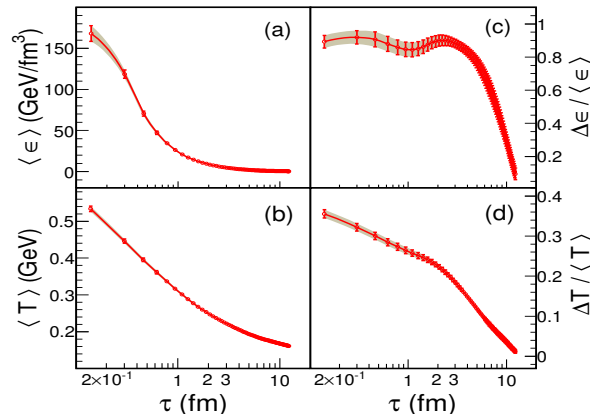


Figure 14. Temporal evolution of (a) average energy density, (b) average temperature, (c) fluctuations in energy density, and (d) fluctuations in temperature for central Pb–Pb collisions at LHC energies obtained from hydrodynamic calculations [48].

is slow till freeze-out. The fall of T with τ is rather smooth. At early times, the fluctuations are observed to be very large, and then decrease rapidly. It is thus clear that a detailed insight into the evolution of fluctuations is possible by studying local fluctuations in ϵ and T .

9. Summary and outlook

In this article, we have discussed a number of fluctuation techniques for understanding the nature of the QCD phase transition over a wide range of baryon chemical potential as well as to locate the critical point. One of the first fluctuation studies is in terms of event-by-event fluctuations of higher-order cumulants of conserved quantities, both diagonal and off-diagonal elements. A comparison with lattice and HRG model calculations provide measures of the freeze-out conditions. Assuming that the signal at freeze-out survives dissipation during the

evolution of the fireball from the hadronization stage, the higher cumulants can be used as one of the preferred tools for locating the critical point. The products of the cumulants are observed to have smooth variation as a function of collision energy for net-charge, net-kaon, and net- Λ distributions. But the experimental results of $\kappa\sigma^2$ at RHIC energies show a sign of non-monotonic behavior in the net-proton multiplicity distributions. We look forward to getting the confirmation of the critical point with future higher statistics data for higher order cumulants of conserved quantities as well as more differential measurements in rapidity and p_T .

We have discussed fluctuations in particle multiplicity, mean transverse momentum ($\langle p_T \rangle$) and temperature to extract isothermal compressibility, specific heat, and the speed of sound. These observables, being sensitive to the phase transition, provide important measures for the nature of the transition and to locate the critical point. Charge-neutral fluctuations in the pion and kaon sectors are discussed in terms of providing signatures of the formation of disoriented chiral condensates. Another topic in terms of fluctuation is to construct local fluctuation maps in rapidity and azimuthal bins. By making a correspondence of measured fluctuations with the time evolution of the fluctuations from theoretical calculations, it is possible to infer the thermodynamic conditions at different stages of the QGP evolution. Most of the fluctuation studies require large coverage of the detectors and large statistics measurements. The STAR experiment with RHIC BES-II is ideal for the search of the critical point. The next-generation multipurpose detector at the LHC as a follow-up to the present ALICE experiment will have a large coverage, which will be suitable for event-by-event fluctuations [49] to probe critical fluctuations at $\mu_B=0$.

10. References

- [1] K. Fukushima, T. Hatsuda, Rept. Prog. Phys. **74**, 014001 (2011).
- [2] C. Ratti, Rept. Prog. Phys. **81**, 084301 (2018).
- [3] Y. Aoki, G. Endrodi, Z. Fodor, S.D. Katz and K.J. Szabo, Nature **443**, 675 (2006).
- [4] M. A. Stephanov, Prog. Theo. Phys. Sup. 153, 139 (2004); Int. J. Mod. Phys. A **20**, 4387 (2005).
- [5] S. Ejiri, Phys. Rev. D **78**, 074507 (2008).
- [6] C. Herold, M. Nahrgang, I. Mithustein and M. Bleicher, Nucl. Phys. A **925**, 14 (2014).
- [7] M.M. Aggarwal *et al.* (STAR Collaboration), arXiv:1007.2613.
- [8] A. Bzdak, S. Esumi, V. Koch, J. Liao, M. Stephanov, N. Xu, Phys. Rep. **853**, 1 (2020).
- [9] M. Stephanov, K. Rajagopal, and E. Shuryak, Phys. Rev. D **60**, 114028 (1999).
- [10] H. Heiselberg, Phys. Rept. **351**, 161 (2001).
- [11] F. Karsch, S. Ejiri, K. Redlich, Nucl. Phys. A **774**, 619(2006).
- [12] L.D. Landau and E.M. Lifshitz, Statistical Physics, v.5, 3rd, rev. and enlarged ed.) Pergamon Press (1980).
- [13] L. Stodolsky, Phys. Rev. Lett. **75**, 1044 (1995).
- [14] S. Mrowczynski, Phys. Lett. B **430** (1998) 9.
- [15] G. Giacalone, F.G. Gardim, J. Noronha-Hostler, and J-Y Ollitrault, arXiv:2004.09799 [nucl-th].
- [16] C. Athanasiou, K. Rajagopal, and M. Stephanov, Phys. Rev. D **82**, 074008 (2010).
- [17] M.A. Stephanov, Phys. Rev. Lett. **102**, 032301 (2009).
- [18] V. Koch, A. Majumder and J. Randrup, Phys. Rev. Lett. **95** 182301 (2005).
- [19] A. Majumder and B Muller, Phys. Rev. C **74**, 054901 (2006).
- [20] R. V. Gavai, Sourendu Gupta, Phys. Rev. D **73**, 014004 (2006).
- [21] A. Chatterjee, S. Chatterjee, T.K. Nayak, N.R. Sahoo, Jour. Phys. G **43**, 125103 (2016).
- [22] J. D. Bjorken, Acta Phys. Polon. B **28**, 2773 (1997).
- [23] K. Rajagopal and F. Wilczek, Nucl. Phys. B **399**, 395 (1993).
- [24] U. Heinz, J. Phys.: Conf. Ser. **455**, 012044 (2013).
- [25] H. Holopainen, H. Niemi, and K. Eskola, Phys. Rev. C **83**, 034901 (2011).
- [26] S. Floerchinger, U.A. Wiedemann, Phys. Rev. C **88**, 044906 (2013).
- [27] M. Mukherjee, S. Basu, A. Chatterjee, S. Chatterjee, S. Adhya, S. Thakur, T. Nayak, Phys. Lett. B **784**, 1 (2018).
- [28] S. Basu, S. Chatterjee, R. Chatterjee, B. Nandi, and T.K. Nayak, Phys. Rev. C **94**, 044901 (2016).
- [29] B. I. Abelev *et al.* (ALICE Collaboration), Phys. Rev. Lett. **110**, 152301 (2013).
- [30] B. I. Abelev *et al.* (STAR Collaboration), Phys. Rev. C **79**, 024906 (2009).
- [31] S. Pratt and C. Plumberg, arXiv:1904.11459 [nucl-th].

- [32] E.V.Shuryak,M.A.Stephanov, Phys. Rev. C **63**, 064903 (2001).
- [33] M. A. Aziz, S. Gavin, Phys. Rev. C **70**, 034905 (2004).
- [34] B. Sharma, M.M. Aggarwal, N.R. Sahoo, T.K. Nayak, Phys. Rev. C. **91**, 024909 (2015).
- [35] L. Adamczyk *et al.* (STAR Collaboration), Phys. Rev. Lett. **113**, 092301 (2014).
- [36] L. Adamczyk *et al.* (STAR Collaboration), Phys. Lett. B **785**, 551 (2018).
- [37] J. Adam *et al.* (STAR Collaboration), arXiv:2001.02852 [nucl-ex].
- [38] M. M. Aggarwal *et al.* (STAR Collaboration), Phys. Rev. Lett. **105**, 022302 (2010).
- [39] L. Adamczyk *et al.* (STAR Collaboration), Phys. Rev. Lett. **112**, 032302 (2014).
- [40] J. Adam *et al.* (STAR Collaboration), arXiv:2001.06419 [nucl-ex].
- [41] J. Adam *et al.* (STAR Collaboration), Phys. Rev.C **100**, 014902 (2019).
- [42] T.K. Nayak *et al.* (WA98 Collaboration), Nucl. Phys. A**638**, 249c (1998).
- [43] M.M. Aggarwal *et al.* (WA98 Collaboration), Phys. Lett. B 420, 169 (1998).
- [44] M.M. Aggarwal *et al.* (WA98 Collaboration), Phys. Rev. C64, 011901 (2001).
- [45] M.M. Aggarwal *et al.* (WA98 Collaboration), Phys. Rev. C67, 044901(2003).
- [46] L. Adamczyk *et al.* (STAR Collaboration), Phys. Rev. C91,034905 (2015).
- [47] R. Nayak, S. Dash, B. Nandi, and C. Pruneau, Phys. Rev. C **101**, 054904 (2020)
- [48] S. Basu, R. Chatterjee, B.K. Nandi, T.K. Nayak, arXiv:1504.04502 [nucl-ex].
- [49] D. Adamova *et al.* arXiv:1902.01211 [physics.ins-det].